# On the Influence of DC Electric Fields on the Aerosol Assisted Chemical Vapor Deposition Growth of Photoactive Titanium Dioxide Thin Films

**ARTICLE** *in* LANGMUIR · OCTOBER 2013

Impact Factor: 4.46 · DOI: 10.1021/la403070b · Source: PubMed



**2 AUTHORS:**

Luz Romero
Queen Mary, University of London
**1** PUBLICATION **6** CITATIONS
SEE PROFILE

Russell Binions
Queen Mary, University of London
**107** PUBLICATIONS **1,466** CITATIONS
SEE PROFILE

Langmuir

Article

pubs.acs.org/Langmuir

# On the Influence of DC Electric Fields on the Aerosol Assisted Chemical Vapor Deposition Growth of Photoactive Titanium Dioxide Thin Films

Luz Romero and Russell Binions*

School of Engineering and Materials Science, Queen Mary University of London, Mile End Road, London E1 4NS, United Kingdom

**ABSTRACT:** Titanium dioxide thin films were deposited on fluorine doped tin oxide glass substrate from the electric field assisted aerosol chemical vapor deposition (EACVD) reaction of titanium isopropoxide (TTIP, $Ti(OC_3H_7)_4$) in toluene on glass substrates at a temperature of 450 °C. DC electric fields were generated by applying a potential difference between the electrodes of the transparent coated oxide coated glass substrates during the deposition. The deposited films were characterized using scanning electron microscopy, X-ray diffraction, atomic force microscopy, Raman spectroscopy, and UV−vis spectroscopy. The photoactivity and hydrophilicity of the deposited films were also analyzed using a dye-ink test and water-contact angle measurements. The characterization work revealed that the incorporation of DC electric fields produced significant reproducible changes in the film microstructure, preferred crystallographic orientation, roughness, and film thickness. Photocatalytic activity was calculated from the half-time ($t_{1/2}$) or time taken to degrade 50% of the initial resazurin dye concentration. A large improvement in photocatalytic activity was observed for films deposited using an electric field with a strong orientation in the (004) direction ($t_{1/2}$ 17 min) as compared to a film deposited with no electric field ($t_{1/2}$ 40 min).

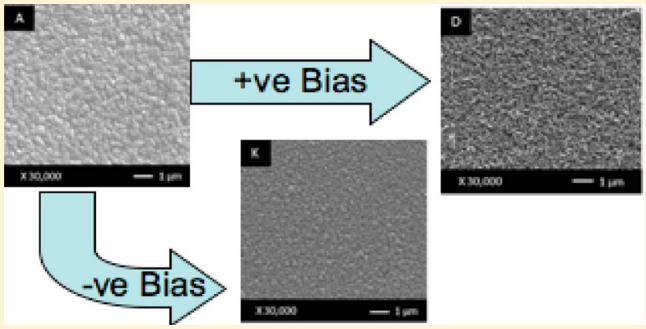


## 1. INTRODUCTION

Titanium dioxide has been the subject of intensive research due to its high suitability as photocatalytic material.[1] Continuing efforts are being made to improve the photocatalytic properties of titania by modifying the microstructure of the material using a variety of methods including sol−gel,[2,3] physical vapor deposition,[4] electrodeposition,[5] and a variety of chemical vapor deposition (CVD) methods such as aerosol assisted CVD (AACVD),[6] atmospheric pressure CVD (APCVD),[7] low pressure CVD,[8] and metal organic (MO) CVD.[9] Among them, CVD has been proven as an excellent method to produce titania thin films due to its advantageous properties such as good conformal coverage, ability to control crystal structure, surface morphology, and orientation, among many others.[10]

In recent years, a number of studies on the effect of electric fields during the CVD growth of different metal oxides have been conducted. In particular, studies on the electric field assisted CVD (EACVD) growth of tungsten oxide thin films showed that electric fields encouraged film thickness and produced changes in morphology, which improved the gas sensing properties of the material.[11,12] Likewise, studies on the EACVD growth of $TiO_2$ thin films demonstrated that the application of electric fields increased the films thickness and decreased the crystallite size as well as changes in crystal orientation, which also increased the gas sensing properties.[13] We have recently shown that titania thin films can be successfully produced from the AC electric field assisted CVD reaction of TTIP in toluene for photocatalytic applications. It was observed that the photocatalytic properties of titania thin films were shown to rely on a complex of factors such as morphology and size of nanoparticles as well as changes in crystal preferred orientation and growth rate, which can be tailored by varying the field strength.[14]

This Article aims to study the effect of DC electric fields in the production of titania thin films from EACVD and investigates how this affects the structural and photocatalytic properties of the deposited films.

## 2. EXPERIMENTAL SECTION

**Film Synthesis.** The deposition of titanium dioxide thin films was carried out from the DC electric field assisted aerosol chemical vapor deposition (EACVD) reaction of 0.5 mL of titanium tetraisopropoxide (99.99% trace metals, Aldrich) in 10 mL of toluene until the depletion of the precursor; this took 15 ± 2 min. The substrate and top plate were glass sheets (90 mm × 45 mm × 4 mm) coated by a fluorine doped tin oxide layer (FTO, Tec 15 Pilkington) with a gap of 1 cm between them as reported previously.[14] The aerosol was produced using a Vicks ultrasonic humidifier, introducing the carrier gas flow once the mist had formed. The carrier gas used was $N_2$ (99.9% BOC) in a flow rate of 2 L $min^{-1}$. The carrier gas transported the precursors to cylindrical quartz cold wall reactor with dimensions of 6 cm diameter and 17 cm length. The temperature of the reactor was set at

**Received:** August 8, 2013
**Revised:** September 23, 2013
**Published:** October 7, 2013

450 °C by heating a graphite block containing a Whatman heating cartridge, which was controlled by a Pt−Rh thermocouple. An electric field was generated by applying a potential difference across the electrodes and regulated from a variable voltage supply unit between 0 and 30 V (Table 1). Depositions were repeated at least twice and fully characterized to check and ensure the reproducibility of the system. An area of 2 × 5 cm in the center of the glass substrate was found to have even growth, and this is the area that was subsequently selected for materials characterization.

**Table 1. Experimental Conditions of Deposited Films from the AACVD Reaction of 0.5 mL of TTIP in 10 mL of Toluene at 450 °C and Gas Flow Rate of 2 L min$^{-1}$ with an Applied DC Electric Field**

| sample | applied voltage (V) | field strength (V m$^{-1}$) | substrate bias | material phase (XRD/EDAX/Raman) |
|---|---|---|---|---|
| A | 0 | 0 | | anatase $TiO_2$ |
| B | 1 | $1 \times 10^2$ | positive | anatase $TiO_2$ |
| C | 5 | $5 \times 10^2$ | positive | anatase $TiO_2$ |
| D | 10 | $10 \times 10^2$ | positive | anatase $TiO_2$ |
| E | 20 | $20 \times 10^2$ | positive | anatase $TiO_2$ |
| F | 30 | $30 \times 10^2$ | positive | anatase $TiO_2$ |
| G | 1 | $1 \times 10^2$ | negative | anatase $TiO_2$ |
| H | 5 | $5 \times 10^2$ | negative | anatase $TiO_2$ |
| I | 10 | $10 \times 10^2$ | negative | anatase $TiO_2$ |
| J | 20 | $20 \times 10^2$ | negative | anatase $TiO_2$ |
| K | 30 | $30 \times 10^2$ | negative | anatase $TiO_2$ |

**Materials Characterization.** Scanning electron microscopy (SEM) was completed using a FEI Inspect F scanning electron microscope. X-ray diffraction (XRD) analysis was conducted using Siemens D5000 (Karlsruhe, Germany) with $Cu_{K\alpha 1}$X-ray source in grazing incidence mode. Raman spectroscopy was carried out using a Renishaw (UK) Raman system 1000 with a helium neon laser of wavelength 514.5 nm. Atomic force microscopy (AFM) analysis was completed using NT-MDT NTEGRA (Zelenograd, Moscow). Semi-contact mode imaging was performed under ambient conditions in air using silicon tips (Acta-20-Appnano ACT tapping mode with aluminum reflex coating, Nanoscience instruments) with a resonant frequency of 300 kHz and a spring constant of 40 N/m. Scan resolution was 256 samples per line. Images were processed and analyzed by the offline software Nova 1.0.26.1443. UV/vis spectroscopy was conducted using a Perkin-Elmer Lambda 950 UV/vis spectrometer. Film thickness was calculated from SEM cross-sectional images electing at least eight different points along the sample and applying a standard error (SE), which was found to vary from 0.009% to 0.4%. Band gaps were calculated using the Tauc method.[15] The agglomerate size was calculated using Image J and by applying SE, which was found to vary from $5 \times 10^{-4}$% to $3 \times 10^{-3}$%.

**Properties Characterization.** Photocatalytic behavior was monitored using an intelligent ink based on the dye Resazurin (Rz).[16−18] The ink was made up of 40 mL of deionized water, 3 g of a 1.5 wt % aqueous solution of hydroxyethyl cellulose (HEC) polymer (Aldrich), 0.3 g of glycerol (Aldrich), and 4 mg of Rz (Aldrich). The titania thin films formed on glass at 450 °C were sprayed with the ink solution using an aerosol spray gun and subsequently irradiated with a 365 nm lamp. In the first instance, the photocatalytic reduction was monitored via digital photographic methods. The dye-coated films changed color from blue (photoreduction of Rz) to pink (Rezofurin). Further photodegradation of the dye produces a colorless state, indicating the total reduction of rezofurin. More accurate measurements were subsequently made using UV/vis spectroscopy and monitoring the reduction of a dye absorption peak at 630 nm using a Perkin-Elmer Lambda 25 instrument. To study the wetting characteristics of the deposited films, water-contact angle measurements before and after 30 min of irradiation with 254 nm light were carried out using a Goniometer Kruss DSA100 drop shape analyzer.

## 3. RESULTS

**3.1. Film Synthesis and Characterization.** The electric field assisted chemical vapor deposition (EACVD) from the reaction of titanium tetraisopropoxide (TTIP) in toluene at 450 °C under the influence of DC electric fields produced anatase $TiO_2$ thin films as confirmed by XRD, EDAX, and Raman spectroscopy (Table 1). Deposited films presented good adherence to the substrate passing the Scotch tape test and a scratch test using a piece of towel. The films produced with DC

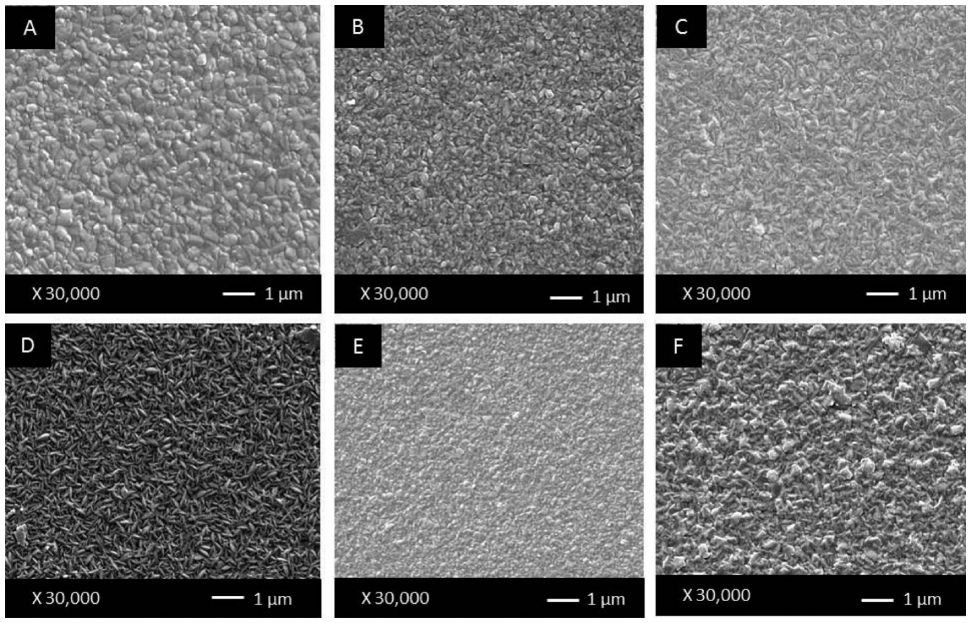


**Figure 1.** Scanning electron microscope images of samples prepared without electric field (sample A) and from the positive biased EACVD reaction (samples B−F) of 0.5 mL of TTIP solution in toluene at 450 °C with a flow rate of 2 L min$^{-1}$. Sample A, 0 V m$^{-1}$; sample B, $1 \times 10^2$ V m$^{-1}$; sample C, $5 \times 10^2$ V m$^{-1}$; sample D, $10 \times 10^2$ V m$^{-1}$; sample E, $20 \times 10^2$ V m$^{-1}$; and sample F, $30 \times 10^2$ V m$^{-1}$.


dx.doi.org/10.1021/la403070b | Langmuir 2013, 29, 13542−13550

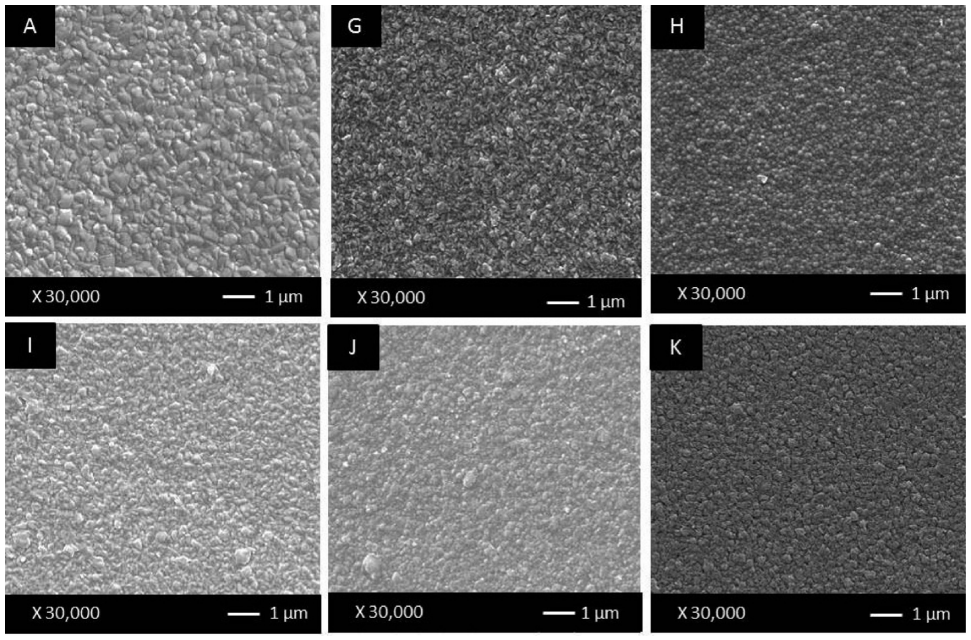


**Figure 2.** Scanning electron microscope images of samples prepared from the EACVD reaction of 0.5 mL of TTIP solution in toluene at 450 °C with a flow rate of 2 L $m^{-1}$. The images correspond to the DC field samples with negative substrate bias: sample A, 0 V $m^{-1}$; sample G, 1 × $10^2$ V $m^{-1}$; sample H, 5 × $10^2$ V $m^{-1}$; sample I, 10 × $10^2$ V $m^{-1}$; sample J, 20 × $10^2$ V $m^{-1}$; sample K, 30 × $10^2$ V $m^{-1}$.

electric fields showed carbon deposition across the surface with the exception of two samples (samples I and K), which, as the film produced with no electric field, were transparent. Nevertheless, all films showed birefringence, indicating different thickness across the surfaces.

Scanning electron microscopy (SEM) images of the deposited titanium dioxide films are shown in Figures 1 (DC positive substrate bias) and 2 (DC negative substrate bias). Deposition carried out in the absence of an electric field (Figure 1A) revealed a thin film comprised of an agglomerated spherical microstructure of 400 nm particle size and thickness of 430 nm. The introduction and increase of a positive biased potential difference across the electrodes of the glass substrate during the AACVD deposition produced a change of morphology and a reduction of particle size as well as variations in the thickness of the deposited films. Thus, at low field strength (1 × $10^2$ to 5 × $10^2$ V $m^{-1}$), the morphology of deposited films changed to elongated microstructure of 200−330 nm length and 100 nm width (Figure 1B,C) with secondary growth of spherical submicronic particles of 340 nm (sample B) and 160 nm (sample C). In this range of field strength, an increase in thickness is produced to 750−800 nm. When the field strength was increased (10 × $10^2$ V $m^{-1}$), the secondary spherical microstructure changed to a rice-like microstructure of 360 nm length and 130 nm width (Figure 1D), and the thickness was increased to 1570 nm. As the field strength was increased to 2 × $10^3$ V $m^{-1}$, the size of the elongated growths decreased to 100 nm length and 50 nm width, forming spherical agglomerations of 150 nm length (Figure 1E). The film thickness deposited at this field strength was higher at 1300 nm. Likewise, films deposited at 30 × $10^2$ V $m^{-1}$ showed elongated growths of 280 nm length and 100 nm width forming spherical agglomerations of 300 nm diameter (Figure 1F). The film thickness at this field strength decreased to 1270 nm.

Changing the film bias from a positive bias (Figure 1) to a negative bias (Figure 2) led to further microstructural and thickness changes. As was observed for depositions from positively biased electric fields, the introduction of negatively biased electric fields (1 × $10^2$ V $m^{-1}$) led to a change of the shape from spherical to elongated particles and decrease in particle size to 250 nm length and 100 nm width (Figure 2G) as well as an increase in film thickness to 600 nm. As the field strength was further increased, continuous changes occurred to the deposited films. Thus, at 5 × $10^2$ V $m^{1-}$ (Figure 2H), the deposited thin films showed spherical growths of 130 nm in diameter and a marked increase in film thickness to 1100 nm. A further increase in field strength (10 × $10^2$ V $m^{-1}$) produced a change in growth to elongated nanoparticles 250 nm in length and 90 nm in width (Figure 2I) as well as an increase of film thickness to 1170 nm. At 20 × $10^2$ V $m^{-1}$, the shape of nanoparticles changed back to spherical with a reduction in particle size to 200 nm (Figure 2J), and the film thickness was significantly reduced to 750 nm. Finally, at 3 × $10^3$ V $m^{-1}$, deposited films revealed a particular morphology pattern identifying elongated microstructures of reduced particle size (140 × 50 nm) forming spherical agglomerations (Figure 2K) with a film thickness of 480 nm.

The results obtained in film thickness indicated a similar growth rate pattern for both positive and negative biased electric fields (Figure 3, Table 3). The increase of the field strength to 10 × $10^2$ V $m^{-1}$ also produced an increase in film thickness, which was more accentuated in positive biased deposited films. From that field strength to 30 × $10^2$ V $m^{-1}$, a gradual decrease in film thickness is produced, which was more accentuated in negative biased deposited films.

X-ray diffraction (XRD) analysis was carried out and compared to previous investigations (JCPDS database file (021-1272)) to study the materials phase. All deposited films under the influence of electric fields showed anatase $TiO_2$ crystalline phase and also cassiterite $SnO_2$ from the FTO glass substrate. The relative intensity of the Bragg peaks associated with $TiO_2$ changed depending on the substrate bias applied, revealing a preferred orientation. Thus, deposited films


dx.doi.org/10.1021/la403070b | Langmuir 2013, 29, 13542−13550

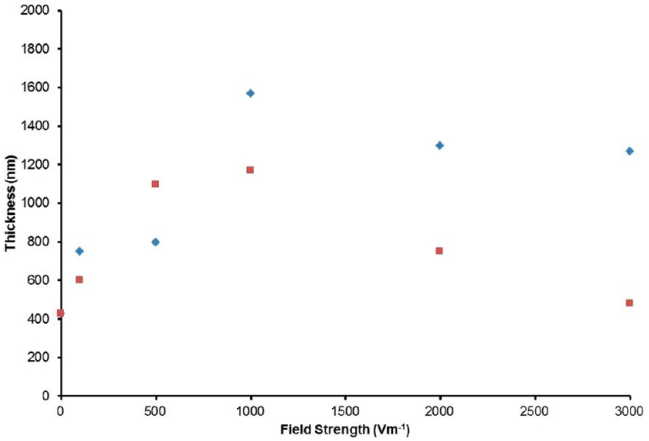


**Figure 3.** Field strength versus film thickness (nm) for positive (◆) and negative bias (■).

prepared with no electric field and films prepared with positive biased electric field showed an apparent crystallographic preferential orientation in the (101) (Figure 4). However, as negative biased electric field is introduced, an apparent change in the crystal orientation is produced in the (004) plane (Figure 5).

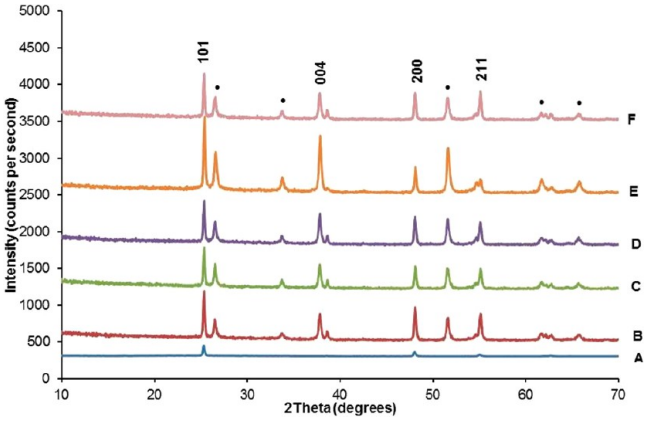


**Figure 4.** XRD pattern for samples prepared without applied electric field (sample A) and from the positive biased EACVD (samples B–F) reaction of 0.5 mL of TTIP in toluene at 450 °C and a gas flow rate of 2 L $min^{-1}$. Sample A, 0 V $m^{-1}$; sample B, 1 × $10^2$ V $m^{-1}$; sample C, 5 × $10^2$ V $m^{-1}$; sample D, 10 × $10^2$ V $m^{-1}$; sample E, 20 × $10^2$ V $m^{-1}$; sample F, 30 × $10^2$ V $m^{-1}$. The peaks marked with dots denote the cassiterite peaks specific to the $SnO_2$ crystalline phase, material used for the glass substrate coating.

Texture coefficient calculations were carried out to confirm the preferred crystal orientation found in XRD analysis.[19] The results (shown in Table 2) revealed that the film produced with no electric field was slightly oriented in the (200) plane as previously reported.[14] Contradictory to the XRD results, thin films produced with positive biased electric fields showed crystal preferred orientation in the (211) plane (samples B and F) and in the (004) plane (samples C–E). The films produced with negative biased electric fields showed crystal preferred orientation in the (004) plane (samples G–K). However, as Table 2 reveals, thin films produced from negative biased electric fields showed higher texture coefficients in the (004) plane than thin films produced from positive biased electric fields.

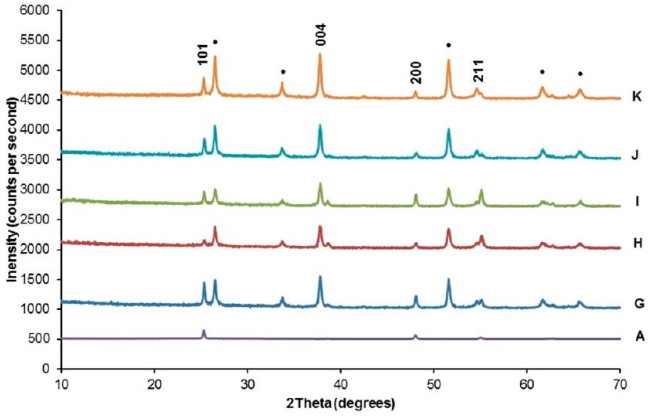


**Figure 5.** XRD pattern for samples prepared without applied electric field (sample A) and from the negative biased EACVD (samples H–M) reaction of 0.5 mL of TTIP in toluene at 450 °C and a gas flow rate of 2 L $min^{-1}$. Sample A, 0 V $m^{-1}$; sample G, 1 × $10^2$ V $m^{-1}$; sample H, 5 × $10^2$ V $m^{-1}$; sample I, 10 × $10^2$ V $m^{-1}$; sample J, 20 × $10^2$ V $m^{-1}$; sample K, 30 × $10^2$ V $m^{-1}$. The peaks marked with dots denote the cassiterite peaks specific to the $SnO_2$ crystalline phase, material used for the glass substrate coating.

**Table 2. Texture Coefficient of $TiO_2$ Thin Films Produced from the AACVD Reaction of TTIP in Toluene at 450 °C with an Applied Electric Field of (A) 0 V $m^{-1}$, (B) +1 × $10^2$ V $m^{-1}$, (C) +5 × $10^2$ V $m^{-1}$, (D) +10 × $10^2$ V $m^{-1}$, (E) +20 × $10^2$ V $m^{-1}$, (F) +30 × $10^2$ V $m^{-1}$, (G) −1 × $10^2$ V $m^{-1}$, (H) −5 × $10^2$ V $m^{-1}$, (I) −10 × $10^2$ V $m^{-1}$, (J) −20 × $10^2$ V $m^{-1}$, and (K) −30 × $10^2$ V $m^{-1}$**

| | texture coefficient ($TC_{hkl}$) | | | |
|---|---|---|---|---|
| sample | (101) | (004) | (211) | (200) |
| A | 1.31 | 0.28 | 1.29 | 1.58 |
| B | 0.48 | 1.27 | 1.32 | 0.93 |
| C | 0.49 | 1.47 | 1.24 | 0.79 |
| D | 0.44 | 1.57 | 1.15 | 0.83 |
| E | 0.58 | 2.22 | 0.58 | 0.60 |
| F | 0.45 | 1.34 | 1.42 | 0.78 |
| G | 0.37 | 2.36 | 0.71 | 0.55 |
| H | 0.17 | 2.21 | 1.29 | 0.32 |
| I | 0.24 | 1.84 | 1.36 | 0.54 |
| J | 0.32 | 2.64 | 0.72 | 0.30 |
| K | 0.26 | 2.75 | 0.70 | 0.28 |

Furthermore, XRD analysis of full width at half-maximum (fwhm) was carried out using the Scherrer equation to investigate the crystallite size of deposited films. Characteristic peaks of 2Θ = 25.28° (101), 2Θ = 37.8° (004), and 2Θ = 48.05° (200) were selected, and the generally used shape factor of 0.9[20] was chosen. As Table 3 shows, the application of DC electric fields produces an increase of the crystallite size as compared to the film produced with no electric field. Although broadly speaking the crystallite size was similar for both positive and negative biased thin films, it was found to have a smaller crystallite size for samples H and K (20 and 21 nm, respectively).

Raman spectroscopy was carried out to complement XRD analysis for phase identification. Figure 6 shows representative Raman spectra for all of the deposited films. The samples gave strong Raman centered at 147, 198, 395, 513, and 642 $cm^{-1}$, which is in accordance with previous studies.[21]


dx.doi.org/10.1021/la403070b | Langmuir 2013, 29, 13542–13550

Table 3. Table of Samples Indicating Particle Size (nm) Measured Using Image J, Crystal Preferred Orientation Calculated from the Texture Coefficient ($TC_{(hkl)}$), Crystallite Size (nm) Calculated by the Scherrer Equation, Film Thickness (nm) Calculated from the SEM Cross Section, Growth Rate (nm $min^{-1}$) Obtained by Dividing the Film Thickness by the Time of Reaction (15 min), and Surface Roughness Calculated from Root Mean Square (RMS) Values Using AFM[a]

| | | agglomerate size | | | | | | |
|---|---|---|---|---|---|---|---|---|
| sample | field strength ($V\ m^{-1}$) | $L$ (nm) | $W$ (nm) | crystal preferred orientation | crystallite size (nm) | film thickness (nm) | growth rate (nm $min^{-1}$) | surface roughness (RMS, nm) |
| A | 0 | 400 | 400 | (200) | 19 | 430 | 28.7 | 115 |
| B | $+1 \times 10^2$ | 200 | 100 | (211) | 27 | 750 | 50.0 | 260 |
| C | $+5 \times 10^2$ | 330 | 100 | (004) | 25 | 800 | 53.3 | 130 |
| D | $+10 \times 10^2$ | 360 | 100 | (004) | 27 | 1570 | 104.7 | 160 |
| E | $+20 \times 10^2$ | 100 | 50 | (004) | 32 | 1300 | 86.7 | 80 |
| F | $+30 \times 10^2$ | 280 | 100 | (211) | 29 | 1270 | 84.7 | 130 |
| G | $-1 \times 10^2$ | 250 | 100 | (004) | 29 | 600 | 40.0 | 250 |
| H | $-5 \times 10^2$ | 130 | 130 | (004) | 20 | 1100 | 73.3 | 120 |
| I | $-10 \times 10^2$ | 250 | 90 | (004) | 29 | 1170 | 78.0 | 100 |
| J | $-20 \times 10^2$ | 200 | 200 | (004) | 24 | 750 | 50.0 | 130 |
| K | $-30 \times 10^2$ | 140 | 50 | (004) | 21 | 480 | 32.0 | 340 |

[a]The signs "+" and "−" in the field strength column indicate the substrate bias.

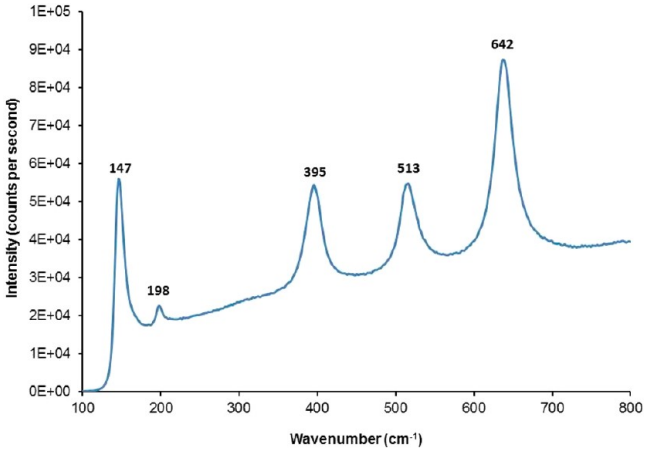


Figure 6. Typical Raman scattering for titanium dioxide sample produced by EACVD (sample K, prepared with a positive bias of $3 \times 10^3$ V $m^{-1}$).

Deposited films surfaces were scanned using AFM over a 20 $\mu$m × 20 $\mu$m region with height variations of ca. 180 nm for deposited film with no electric field, 400 nm to 1.2 $\mu$m for positive biased deposited films, and 450−900 nm for negative biased deposited films. Figure 8 shows AFM images for samples A (0 V $m^{-1}$), C ($+5 \times 10^2$ V $m^{-1}$), and F ($+30 \times 10^2$ V $m^{-1}$). Furthermore, root mean square (RMS) values were calculated as a proxy of surface roughness (Table 3). It was observed that the application of DC field strength increased the roughness of surfaces from 115 to 260 nm (DC +ve) and to 250 nm (DC −ve). As positive biased field strength was increased (samples C and D), the roughness decreased (130−160 nm) but still remained greater than the film deposited with no electric field. At $+2 \times 10^3$ V $m^{-1}$ the roughness decreased dramatically to 80 nm. The increase of negative biased (samples H−J) also decreased the roughness of surfaces to 130 nm but at $-3 \times 10^3$ V $m^{-1}$ the RMS value radically increased to 340 nm.

UV/vis spectroscopy showed that both field strength and substrate bias had an influence on the transmission values over the visible region. Thus, the same increasing pattern in transmission was found for positive and negative biased at lower field strength ($0-10 \times 10^2$ V $m^{-1}$). However, at field strength values greater than $10 \times 10^2$ V $m^{-1}$, transmission of negative biased samples tends to decrease, while in positive biased samples transmittance tended to increase. This can be attributed to the incorporation of carbon into the films, which was found to be more significant with the films deposited with a negative bias. The highest transmission values are found for the thin films prepared with a positive substrate bias and field strength of $20 \times 10^2$ V $m^{-1}$ (78.68%). Band gap analysis was performed using the Tauc method.[15] Field strength seems to have a certain influence on the direct band gap of deposited films. Thus, standard anatase band gap values between 3.2 and 3.3 eV were found for positive and negative biased deposited films. Nevertheless, at higher field strength, lower direct band gap values were found (3.05 eV at $-3 \times 10^3$ V $m^{-1}$ and 3.1 eV at $+20 \times 10^2$ V $m^{-1}$).

**3.2. Functional Properties.** *3.2.1. Photoactivity of $TiO_2$ Thin Films.* The photocatalytic activity of the titania thin films deposited from EACVD was investigated from the UV/vis absorption of Resazurin intelligent ink under UV irradiation (365 nm). It was observed that titania thin films produced under the influence of DC electric fields showed a higher decrease in absorption than the sample produced without electric fields (Figure 8). The time required for the initial dye concentration to decline by one-half ($t_{1/2}$) was calculated for all deposited films (Table 3). The highest value was found for the sample produced with no electric fields (40.1 min), which agreed with previous studies carried out with AC electric fields.[14] It was found that values for $t_{1/2}$ did not decrease remarkably when DC electric fields were applied and were similar among the different field strengths. However, negative biased showed slightly higher photocatalytic activity than positive biased titania thin films. In particular, the most photoactive thin films were sample G (17 min) and sample K (19 min). Nevertheless, it was observed that the application of DC electric fields significantly reduced the photocatalytic activity of titania thin films as compared to AC electric fields in which $t_{1/2}$ values of 2.5 min were found for the most photoactive film.[14]

*3.2.2. Water-Contact Angles.* $TiO_2$ is generally considered to be hydrophilic and frequently superhydrophilic particularly under UV irradiation.[6] It was observed that, under dark conditions, the thin film produced with no electric fields was


dx.doi.org/10.1021/la403070b | Langmuir 2013, 29, 13542−13550

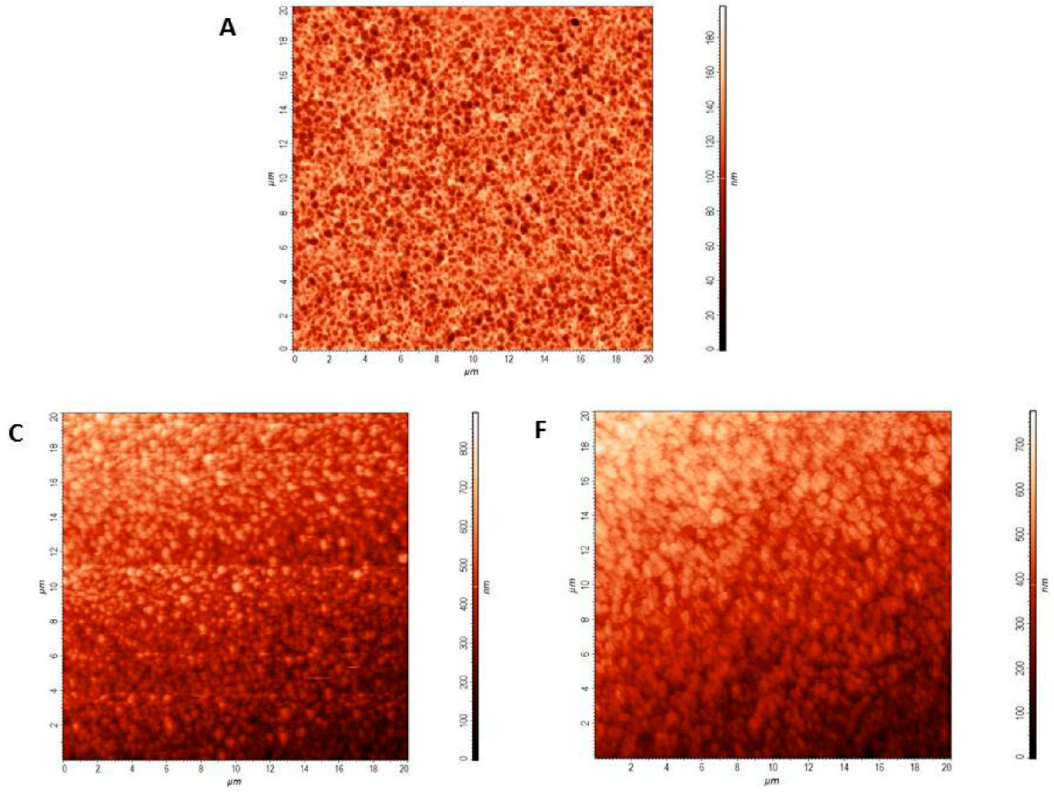


**Figure 7.** Representative AFM images for samples (A) 0 V $m^{-1}$, (C) +5 × $10^2$ V $m^{-1}$, and (F) +30 × $10^2$ V $m^{-1}$.

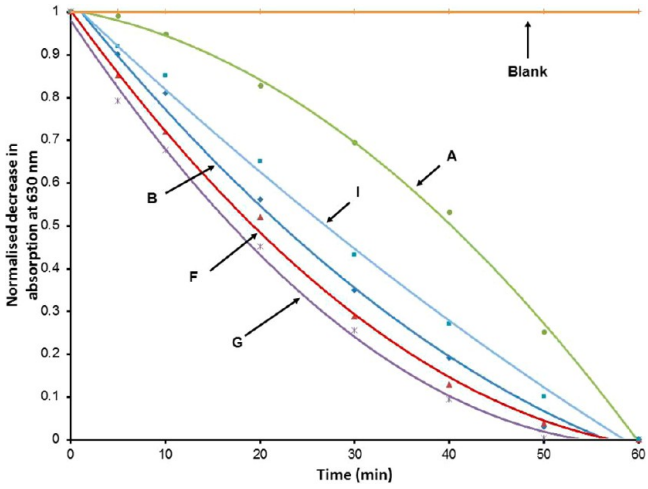


**Figure 8.** Representative normalized decrease in absorption of Resazurin intelligent ink at 630 nm with UVA irradiation (365 nm) against time (A) 0 V $m^{-1}$, (B) +1 × $10^2$ V $m^{-1}$, (F) +30 × $10^2$ V $m^{-1}$, (G) −1 × $10^2$ V $m^{-1}$, and (I) −10 × $10^2$ V $m^{-1}$. A representative graph is depicted for the clarity of the presentation.

hydrophobic with a water-contact angle of 104.7° (Table 4). However, the films from EACVD produced more hydrophilic surfaces with water-contact angles in the range of 83.7°−13.6°. After 30 min of 254 nm UV irradiation, all thin films showed hydrophilicity with contact angles between 46.2° and 5.7°, and in some cases superhydrophilicity with water-contact angles below 5° (samples D−F).

## 4. DISCUSSION

The influence of electric fields in CVD processes has been under investigation in recent years.[12,13,21−24] In particular, studies on the influence of AC electric fields during the CVD deposition of titania thin films have revealed that microstructure characteristics (shape and size of nanoparticles, preferred orientation, and film thickness) can be tailored to achieve good photocatalytic performances.[14]

**Modifications in Microstructure.** We have previously reported how the application of AC electric fields produced changes in the morphology and of microstructure and a decrease in particle size. The application of DC electric fields during the EACVD growth of other materials has been proven to affect the morphology and size of nanoparticles,[24] observing significant changes at higher field strengths. In this work, such changes in the microstructure were also observed with a clear tendency for reduced elongated nanoparticles even at low field strength for both positive and negative bias. This may support the argument that believes that the way the TTIP precursor assembles under the influence of electric fields responds to a substrate effect rather than an interaction between the precursor and the electric field.[12−14] Previous research on the production of tungsten oxide from EACVD for gas sensing purposes[11] showed an increase of deposited material using both AC and DC electric fields. This was attributed to a polarization of aerosol particles whose time-of-flight would be affected by the field strength. However, as it has been already reported, TTIP is an electrically symmetrical precursor.[12,14]

In contrast samples made with AC electric fields, with a direct current the field is always exerted on one constant direction. Thus, DC electric fields would encourage the acceleration toward and nucleation of appropriately charged species on the substrate, which may explain the increase in


dx.doi.org/10.1021/la403070b | Langmuir 2013, 29, 13542−13550

Table 4. Table Showing Thin Film Thickness (nm), Surface Roughness (nm), Water-Contact Angles of Deposited $TiO_2$ Thin Films on Glass Substrate (A) Before and (B) After Irradiation with 254 nm Light for 30 min, and Half-Life Photocatalytic Testing or Time Needed To Degrade 50% of the Ink Initial Concentration, $t_{1/2}$ (min)[a]

| | | | | contact angle (deg) | | photocatalysis testing |
|---|---|---|---|---|---|---|
| sample | field strength (V $m^{-1}$) | thickness (nm) | surface roughness (RMS, nm) | A | B | $t_{1/2}$ (min) |
| A | 0 | 430 | 115 | 104.7 | 21.7 | 40.1 |
| B | $+1 \times 10^2$ | 750 | 260 | 35 | 25.7 | 22.3 |
| C | $+5 \times 10^2$ | 800 | 130 | 25.8 | 8.8 | 20 |
| D | $+10 \times 10^2$ | 1570 | 160 | 25.4 | 4.7 | 21 |
| E | $+20 \times 10^2$ | 1300 | 80 | 13.6 | 3.9 | 20.3 |
| F | $+30 \times 10^2$ | 1270 | 130 | 24.2 | 1.9 | 19.5 |
| G | $-1 \times 10^2$ | 600 | 250 | 24.4 | 16.4 | 17 |
| H | $-5 \times 10^2$ | 1100 | 120 | 63.6 | 28.6 | 21 |
| I | $-10 \times 10^2$ | 1170 | 100 | 61.9 | 5.7 | 27 |
| J | $-20 \times 10^2$ | 750 | 130 | 56.6 | 46.2 | 24 |
| K | $-30 \times 10^2$ | 480 | 340 | 83.7 | 10.6 | 19 |

[a]The signs "+" and "−" in the field strength column indicate the substrate bias.

thickness of deposited materials. Likewise, it would explain the increase in crystallite size and the predominance of elongated nanoparticles, which would undergo a stretching effect when nucleating on the substrate. In particular, negative biased deposited films showed an increasing trend until $10 \times 10^2$ V $m^{-1}$ where the thickness gradually decreased. Positively biased EACVD produced thicker titania thin films formed of larger agglomerates, which indicated that surfaces were more reactive or that the charged species attracted to this surface were more reactive.

The surface effect can be explained in terms of the thermal decomposition mechanism of the TTIP molecule (Ti$(OC_3H_7)_4$) on the substrate. Previous studies suggested that the thermal decomposition of the molecule was produced from the breakdown of Ti−O bonds giving isopropoxy ligand radicals $(OC_3H_7)^*$ at temperatures from 120 to 350 K.[25] At higher temperatures (>890 K), the following pathways were suggested:

$$2Ti{-}OC_3H_7{}^* \rightarrow 2Ti^* + HOC_3H_7 \uparrow + OC_3H_6 \uparrow (\text{at } 890\ \text{K}) \quad (1)$$

$$Ti{-}OC_3H_7{}^* \rightarrow Ti{-}OH^* + C_3H_6 \uparrow (\text{at } 930\ \text{K}) \quad (2)$$

At 890 K, the breakdown of the TTIP molecule gave titanium cations as well as isopropanol and acetone products, which were volatised (reaction 1). At 930 K, the expected reaction 2 under our experimental conditions, the thermal decomposition of TTIP led to the production of titanium hydroxyl groups and propylene. The higher observed thickness of the films deposited with a positively biased surface suggests that reaction 2 is much more likely to be occurring. Thus, the titanium hydroxyl radicals would be attracted to the positively biased surface, increasing the thickness of the deposited titania thin films. The negatively biased surfaces grow more slowly as is evidenced in Figure 3. This would also explain why all of the samples produced with a positive substrate contained carbon contamination; the $C_3H_6$ with high electron density in the double bond would likely be attracted to the positively biased substrate and thus caught up in the growing film. The films produced with a strong electric field and negative substrate bias (samples I and K) would effectively deflect any radicals, negatively charged species, or centers of negative charge away from the substrate surface, accounting for why no carbon is found in the deposited films. The titanium species would still be able to diffuse to the surface, as they would be less affected by the electric field being heavier than the $C_3H_6$ species.

**Changes in Crystallographic Preferred Orientation.** The application and increase of DC electric fields produced a change in the crystal preferred orientation. In the case of positive biased electric fields, the crystal preferred orientation changed from the (200) to the (211) plane and to the (004) at higher field strengths. However, the application and increase of negative biased electric fields caused higher preferred orientation in the (004) plane than positive biased deposited films. Thus, it seems that surface effect is favored with negative biased field strength, which suggests a surface dipole directed growth. The films grown with positively biased surfaces were less textured than the samples grown with the reverse bias. We have previously attributed crystallographic orientation effects as the result of surface dipole direction.[26] The less textured films deposited on the positively biased surfaces give support to this argument. The reactions occurring at the positively biased surface are likely to be quicker (as the implied growth rate is faster); this would mean that any surface dipole effects would be expected to be less prevalent and the subsequently deposited film less textured.

**Effect on Surface Roughness and Water-Contact Angle.** Wettability is governed by surface energy and surface roughness.[27] Numerous authors have tried to explain the relationship between wettability and surface roughness,[28] with the Wenzel[29] and Cassie−Baxter[30] models being the most known. The Wenzel model uses the roughness factor (ratio between the actual surface and geometric surface) to describe the relationship between the apparent contact angle on the rough surface and the Young contact angle. The Cassie−Baxter model is an extension of the Wenzel model considering chemical and physical heterogeneities of surfaces. In this case, the Cassie−Baxter model seems to be more plausible than the Wenzel model. The film produced with no electric field (sample A) showed high surface roughness (RMS = 115 nm) and hydrophobic surfaces under dark conditions (104.7°). The incorporation of DC electric fields produced an increase of surface roughness for all field strengths applied with the exception of samples E and I. Nevertheless, all deposited films showed hydrophilic surfaces under dark conditions with water-contact angles below 90° and even superhydrophilic surfaces after 30 min UVA irradiation (samples D−F). Hence, a


dx.doi.org/10.1021/la403070b | Langmuir 2013, 29, 13542−13550

disparity between water-contact angles and surface roughness was observed accrediting that such a relation also depends on the surface energy.

**Photocatalytic Properties.** We have previously shown that reduction in particle size and change in shape to elongated nanoparticles achieved by tailoring AC field strength positively influenced the photocatalytic activity of the material.[14] This is supported by the results obtained in this work from films deposited with DC electric fields. The best photocatalytic activity result was obtained for sample G ($t_{1/2}$ = 17 min) that showed elongated nanoparticles in their microstructure (Figure 3). Particle size is also known to play an important role in the photocatalytic activity of titania thin film; this is observed for sample K ($t_{1/2}$ = 19 min), which showed a reduced particle size of 140 × 100 nm. It was also observed that the films with highest photocatalytic activity (samples G and K) did not show appreciably high values of film thickness (<1 $\mu$m). Certainly, thick films have been shown to lower the photocatalytic activity of titania thin films due to the difficulty of charged carriers transfer from the bulk of the material to the surface.[31,32] Sample A had a low thickness (430 nm) but displayed poor photocatalytic activity ($t_{1/2}$ = 40.1 min). This is attributed to the preferred orientation in the less favorable (200) plane, whereas the best performing samples (G and K) showed preferred orientation in the (004) plane. Sample G showed higher preferred crystal orientation in the (004) with a texture coefficient value of 2.36. Sample K showed a high texture coefficient (2.75) in the (004) plane and the highest value in surface roughness (RMS = 340 nm) that has previously been proven to enhance the photocatalytic properties of titania due to an increase in surface area.[33] Sample G gave a better photocatalytic performance than sample K due to the fact that its surface wetting is superior (Table 4).

Overall, the best photocatalytic performances were given by films that were strongly orientated in the (004) plane. This effect is suggested to be more important than any other when determining the photocatalytic activity of titania thin films.

## 5. CONCLUSIONS

The application of DC electric fields during the aerosol assisted CVD reaction of titanium isopropoxide in toluene produced titania thin films. The introduction of DC electric fields produced significant alternations in the deposited film morphology, particle size, growth rate, and preferred crystal orientation. These modifications led to significant changes in the photocatalytic properties of the material. In particular, it was observed that factors such as preferred crystal orientation in the 004 plane dominated the photocatalytic activity in comparison to other variables such as shape and particle size or film. In particular, the best photocatalytic performance was achieved by thin films that showed small, elongated nanoparticles (ca. 100 nm) and high orientation in the (004) plane.

## AUTHOR INFORMATION

### Corresponding Author

*E-mail: r.binions@qmul.ac.uk.

### Notes

The authors declare no competing financial interest.

## ACKNOWLEDGMENTS

We would like to thank Dr. Zofia Luklinska, Dr. Rory Wilson, Mr. M. E. A. Warwick, and Miss Charline Sellam for their appreciated assistance in this work.

## REFERENCES

(1) Kazuhito Hasimoto, H. I.; Fujishima, A. TiO2 Photocatalysis: A historical overview and future prospects. *Jpn. J. Appl. Phys.* **2005**, 8269−8285.

(2) Šegota, S.; Ćurković, L.; Ljubas, D.; Svetličić, V.; Houra, I. F.; Tomašić, N. Synthesis, characterization and photocatalytic properties of sol−gel TiO2 films. *Ceram. Int.* **2011**, *37*, 1153−1160.

(3) Malengreaux, C. M.; Timmermans, A.; Pirard, S. L.; Lambert, S. D.; Pirard, J.-P.; Poelman, D.; Heinrichs, B. Optimized deposition of TiO2 thin films produced by a non-aqueous sol−gel method and quantification of their photocatalytic activity. *Chem. Eng. J.* **2012**, *195*−*196*, 347−358.

(4) Tavares, C. J.; Marques, S. M.; Rebouta, L.; Lanceros-Méndez, S.; Sencadas, V.; Costa, C. M.; Alves, E.; Fernandes, A. J. PVD-Grown photocatalytic TiO2 thin films on PVDF substrates for sensors and actuators applications. *Thin Solid Films* **2008**, *517*, 1161−1166.

(5) Ishikawa, Y.; Matsumoto, Y. Electrodeposition of TiO2 photocatalyst into nano-pores of hard alumite. *Electrochim. Acta* **2001**, *46*, 2819−2824.

(6) Edusi, C.; Hyett, G.; Sankar, G.; Parkin, I. P. Aerosol-assisted CVD of titanium dioxide thin films from methanolic solutions of titanium tetraisopropoxide; Substrate and aerosol-selective deposition of rutile or anatase. *Chem. Vap. Deposition* **2011**, *17*, 30−36.

(7) Dunnill, C. W.; Aikin, Z. A.; Pratten, J.; Wilson, M. W.; Parkin, I. N-doped titania thin films, prepared by atmospheric pressure chemical vapour deposition: Enhanced visible light photocatalytic activity and anti-microbial effects. *ECS Trans.* **2009**, *25*, 65−72.

(8) Jung, S.-C.; Kim, S.-J.; Imaishi, N.; Cho, Y.-I. Effect of TiO2 thin film thickness and specific surface area by low-pressure metal−organic chemical vapor deposition on photocatalytic activities. *Appl. Catal., B* **2005**, *55*, 253−257.

(9) Babelon, P.; Dequiedt, A. S.; Mostéfa-Sba, H.; Bourgeois, S.; Sibillot, P.; Sacilotti, M. SEM and XPS studies of titanium dioxide thin films grown by MOCVD. *Thin Solid Films* **1998**, *322*, 63−67.

(10) K. L., C. Chemical vapour deposition of coatings. *Prog. Mater. Sci.* **2003**, *48*, 57−170.

(11) Shaw, G.; Parkin, I. P.; Pratt, K. F. E.; Williams, D. E. Control of semiconducting oxide gas-sensor microstructure by application of an electric field during aerosol-assisted chemical vapour deposition. *J. Mater. Chem.* **2005**, *15*, 149−154.

(12) Naik, A. J. T.; Warwick, M. E. A.; Moniz, S. J. A.; Blackman, C. S.; Parkin, I. P.; Binions, R. Nanostructured tungsten oxide gas sensors prepared by electric field assisted aerosol assisted chemical vapour deposition. *J. Mater. Chem. A* **2013**, *1*, 1827−1833.

(13) Panjawi, N.; Naik, A.; Warwick, M. E. A.; Hyett, G.; Binions, R. The preparation of titanium dioxide gas sensors by the electric field assisted aerosol CVD reaction of titanium isopropoxide in toluene. *Chem. Vap. Deposition* **2012**, *18*, 106.

(14) Romero, L.; Binions, R. Effect of AC electric fields on the aerosol assisted chemical vapour deposition growth of titanium dioxide thin films. *Surf. Coat. Technol.* **2013**, *230*, 196−201.

(15) Tauc, J. Optical properties and electronic structure of amorphous Ge and Si. *Mater. Res. Bull.* **1968**, *3*, 37−46.

(16) Mills, A.; Lepre, A.; Elliott, N.; Bhopal, S.; Parkin, I. P.; O'Neill, S. A. Characterisation of the photocatalyst Pilkington Activ: a reference film photocatalyst? *J. Photochem. Photobiol., A* **2003**, *160*, 213−224.

(17) Kafizas, A.; Adriaens, D.; Mills, A.; Parkin, I. P. Simple method for the rapid simultaneous screening of photocatalytic activity over multiple positions of self-cleaning films. *Phys. Chem. Chem. Phys.* **2009**, *11*, 8367−8375.

(18) Kafizas, A.; Mills, A.; Parkin, I. P. A comprehensive aerosol spray method for the rapid photocatalytic grid area analysis of semi-

conductor photocatalyst thin films. *Anal. Chim. Acta* **2010**, *663*, 69−76.
(19) Saleem, L. F.; Ruan, H. B.; Wu, F.; Huang, Q. L.; Xu, C. L.; Kong, C. Y. Effect of zinc acetate concentration on the structural and optical properties of ZnO thin films deposited by sol-gel method. *Int. J. Phys. Sci.* **2012**, *7*, 2971−2979.
(20) Tayade, R. J.; Kulkarni, P. K. S.; Jasra, R. V. Photocatalytic degradation of dyes and organic contaminants in water using nanocrystalline anatase and rutile TiO2. *Sci. Technol. Adv. Mater.* **2007**, 455−463.
(21) Warwick, M. E. A.; Dunnill, C. W.; Goodall, J.; Darr, J. A.; Binions, R. Hybrid chemical vapour and nanoceramic aerosol assisted deposition for multifunctional nanocomposite thin films. *Thin Solid Films* **2011**, *519*, 5942−5948.
(22) Crane, J.; Warwick, M.; Smith, R.; Furlan, N.; Binions, R. The application of electric fields to aerosol assisted chemical vapor deposition reactions. *J. Electrochem. Soc.* **2011**, *158*, D62−D67.
(23) Warwick, M. E. A.; Binions, C. W. D. Multifunctional nanocomposite thin films by aerosol-assisted CVD. *Chem. Vap. Deposition* **2010**, *16*, 220−224.
(24) Warwick, M. E. A.; Ridley, I.; Binions, R. Electric fields in the chemical vapour deposition growth of vanadium dioxide thin films. *J. Nanosci. Nanotechnol.* **2011**, *11*, 8162.
(25) Cho, S.-I.; Chung, C.-H.; Moon, S. H. Temperature-programmed desorption study on the decomposition mechanism of Ti (OC 3H 7) 4 on Si(100). *J. Electrochem. Soc.* **2001**, *148*, C599−C603.
(26) Naik, A. J. T.; Bowman, C.; Panjwani, N.; Warwick, M. E. A.; Binions, R. Electric field assisted aerosol assisted chemical vapour deposition of nanostructured metal oxide thin films. *Thin Solid Films* **2013**, *544*, 452−456.
(27) Liang, Q.; Chen, Y.; Fan, Y.; Hu, Y.; Wu, Y.; Zhao, Z.; Meng, Q. Tailoring the wettability of nanocrystalline TiO2 films. *Appl. Surf. Sci.* **2012**, *258*, 2266−2269.
(28) Giljean, S.; Bigerelle, M.; Anselme, K.; Haidara, H. New insights on contact angle/roughness dependence on high surface energy materials. *Appl. Surf. Sci.* **2011**, *257*, 9631−9638.
(29) Wenzel, R. N. Resistance of solid surfaces to wetting by water. *Ind. Eng. Chem.* **1936**, *28*, 988−994.
(30) Cassie, S. B. Wettability of porous surfaces. *Trans. Faraday Soc.* **1944**, *40*, 546−551.
(31) Radhiyah Abd Aziz, I. S. Synthesis of TiO2-SiO2 powder and thin film photocatalysts by sol-gel method. *Indian J. Chem., Sect. A* **2009**, *48A*, 951−957.
(32) Hyett, G.; Darr, J. A.; Mills, A.; Parkin, I. P. An investigation into the optimum thickness of titanium dioxide thin films synthesized by using atmospheric pressure chemical vapour deposition for use in photocatalytic water oxidation. *Chem.-Eur. J.* **2010**, *16*, 10546−10552.
(33) Kwon, C. H.; Shin, H.; Kim, J. H.; Choi, W. S.; Yoon, K. H. Degradation of methylene blue via photocatalysis of titanium dioxide. *Mater. Chem. Phys.* **2004**, *86*, 78−82.